Transcriptomics and metabolomics of engineered *Synechococcus elongatus* during photomixotrophic growth

Lin-Rui Tan[1], Yi-Qi Cao[1], Jian-Wei Li[1], Peng-Fei Xia[1] and Shu-Guang Wang[1,2*]

Abstract

Background: Converting carbon dioxide (CO_2) into value-added chemicals using engineered cyanobacteria is a promising strategy to tackle the global warming and energy shortage issues. However, most cyanobacteria are autotrophic and use CO_2 as a sole carbon source, which makes it hard to compete with heterotrophic hosts in either growth or productivity. One strategy to overcome this bottleneck is to introduce sugar utilization pathways to enable photomixotrophic growth with CO_2 and sugar (e.g., glucose and xylose). Advances in engineering mixotrophic cyanobacteria have been obtained, while a systematic interrogation of these engineered strains is missing. This work aimed to fill the gap at omics level.

Results: We first constructed two engineered *Synechococcus elongatus* YQ2-gal and YQ3-xyl capable of utilizing glucose and xylose, respectively. To investigate the metabolic mechanism, transcriptomic and metabolomic analysis were then performed in the engineered photomixotrophic strains YQ2-gal and YQ3-xyl. Transcriptome and metabolome of wild-type *S. elongatus* were set as baselines. Increased abundance of metabolites in glycolysis or pentose phosphate pathway indicated that efficient sugar utilization significantly enhanced carbon flux in *S. elongatus* as expected. However, carbon flux was redirected in strain YQ2-gal as more flowed into fatty acids biosynthesis but less into amino acids. In strain YQ3-xyl, more carbon flux was directed into synthesis of sucrose, glucosamine and acetaldehyde, while less into fatty acids and amino acids. Moreover, photosynthesis and bicarbonate transport could be affected by upregulated genes, while nitrogen transport and assimilation were regulated by less transcript abundance of related genes in strain YQ3-xyl with utilization of xylose.

Conclusions: Our work identified metabolic mechanism in engineered *S. elongatus* during photomixotrophic growth, where regulations of fatty acids metabolism, photosynthesis, bicarbonate transport, nitrogen assimilation and transport are dependent on different sugar utilization. Since photomixotrophic cyanobacteria is regarded as a promising cell factory for bioproduction, this comprehensive understanding of metabolic mechanism of engineered *S. elongatus* during photomixotrophic growth would shed light on the engineering of more efficient and controllable bioproduction systems based on this potential chassis.

Keywords: *Synechococcus elongatus*, Photomixotrophic, Transcriptomics, Metabolomics, Glucose, Xylose

*Correspondence: wsg@sdu.edu.cn
[1] Shandong Key Laboratory of Water Pollution Control and Resource Reuse, School of Environmental Science and Engineering, Shandong University, Qingdao 266237, China
Full list of author information is available at the end of the article

Background

Cyanobacteria are gaining popularity as microbial cell factories due to the capability of directly converting carbon dioxide (CO_2) into value-added products, providing a potential solution for reducing the emission of greenhouse gases and the reliance on fossil fuels [1, 2]. Current

Tan *et al. Microbial Cell Factories* (2022) 21:31

Page 2 of 14

studies showed that a wide spectrum of chemicals, such as alcohols, acids and alkanes, have been successfully produced by engineered cyanobacteria [3]. However, most cyanobacteria (e.g., *Synechococcus elongatus*) can only use inorganic CO_2 as carbon source [4, 5], which inevitably limits the growth and productivity of cyanobacteria and makes it challenging for industrialization.

Two attempts have been made to overcome this challenge in cyanobacteria. One is to improve CO_2 fixation by engineering RuBisCO (ribulose-1,5-bisphosphate carboxylase/oxygenase), the key enzyme in Calvin cycle, for higher carboxylation activity [6–8]. The other is to enable the utilization of organic carbon source (e.g., glucose and xylose) via introducing sugar utilization pathways and allow photomixotrophic growth of cyanobacteria [9]. During growth with light, CO_2 and sugar, the productivity of chemicals and growth of cyanobacteria can be considerably increased. For instance, xylose utilization significantly enhanced growth of cyanobacteria and enabled a 64% increase of ethylene productivity to 9.86 mL/L over photoautotrophic production [10]. Efficient utilization of glucose and CO_2 could increase production of 2,3-butanediol (23BD) to as much as 12.6 g/L in cyanobacteria [11].

As a representative, the model cyanobacterium *Synechococcus elongatus* PCC7942 (hereafter abbreviated as *S. elongatus* unless otherwise specified) has been engineered to utilize organic carbon with CO_2 and sunlight, and has confirmed better performance in growth and productivity [12, 13]. The introduction of sugar utilization pathway allows *S. elongatus* to use glucose or xylose as a supplementary carbon source, therefore increasing the carbon flux and leading to higher production of designed products (e.g., 23BD) or accumulation of biomass [14]. Moreover, increased sugar utilization was investigated to further enhance productivity [11]. Although progresses have been made in this endeavor, the impact of extra carbon on the metabolisms of *S. elongatus* at omics level is still unclear. A systematic analysis of the engineered photomixotrophic cyanobacteria at molecular levels is imperative to further explore the potentials of this synthetic strategy.

Here, we engineered two *S. elongatus* strains YQ2-gal and YQ3-xyl capable of utilizing glucose and xylose, respectively. Transcriptomic and metabolomic analysis were performed in these strains under photomixotrophic condition with corresponded sugar using wild-type *S. elongatus* (WT) under photoautotrophic condition as baselines. Differentially expressed genes (DEGs) and differential metabolites were analyzed to capture the transcriptional perturbations and metabolic changes. Specifically, regulations in carbon metabolic pathways, nitrogen assimilation, membrane transport, fatty acids
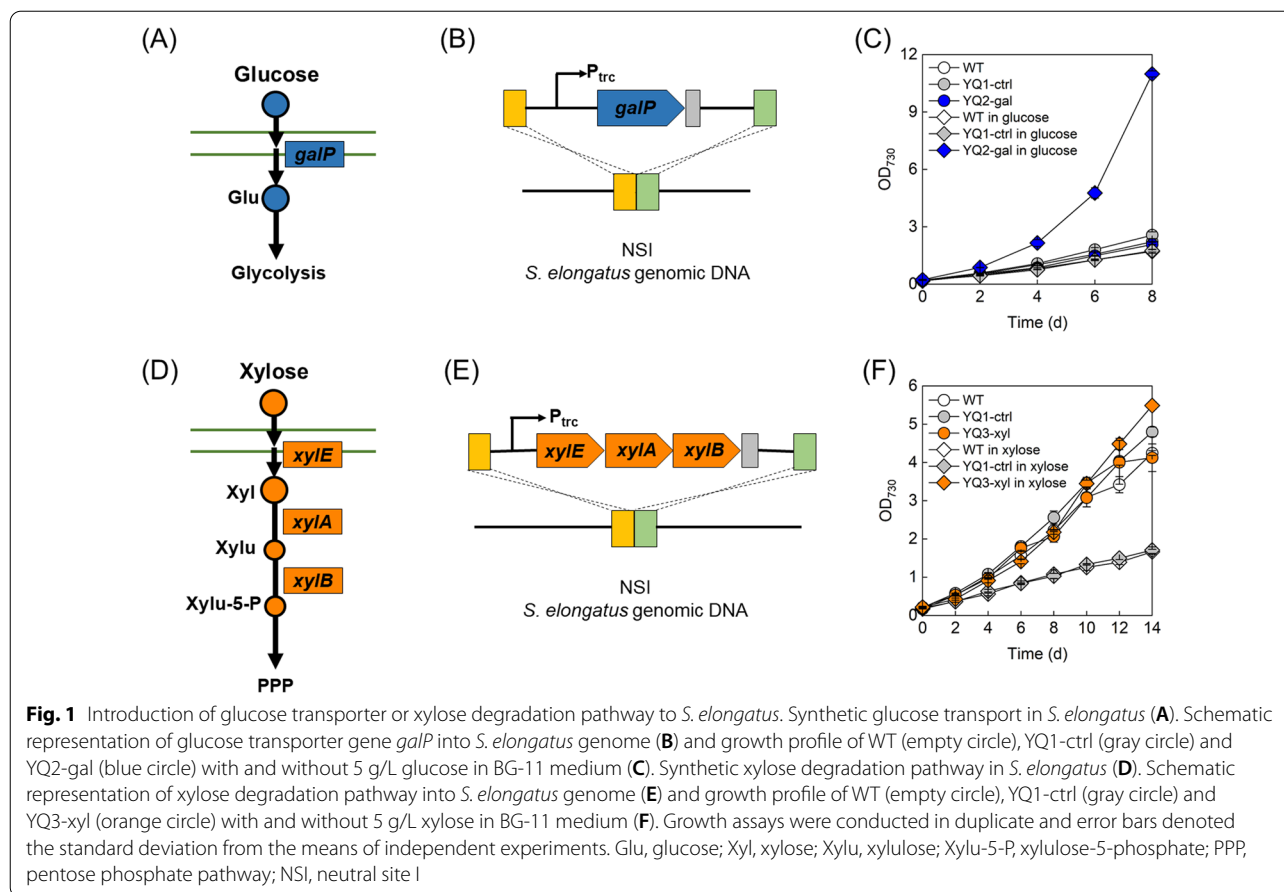
and amino acids biosynthesis were elucidated. Since these metabolic pathways provides precursors or energy for chemical production in cyanobacteria, potential effect of sugar utilization on photomixotrophic bioproduction in engineered *S. elongatus* was further discussed. Our study will fill the gap between metabolic engineering and the biology of synthetic photomixotrophic *S. elongatus*, which will not only provide new insights into the physiology and genetics of cyanobacteria, but also offer guidance to the metabolic engineering of this promising microbial chassis.

Results and discussion
Growth profile of engineered *S. elongatus* with glucose and xylose

It was reported that efficient uptake of glucose is the missing factor that hinders the utilization of glucose in *S. elongatus* (Fig. 1A) [14]. Therefore, an engineered strain harboring a glucose transporter was constructed and denoted as YQ2-gal. Specifically, *galP* gene from *Escherichia coli* was integrated into *S. elongatus* chromosome at neutral site I (NSI) under the control of P_{trc} promoter (Fig. 1B). A strain constructed via same construction process as YQ2-gal but without *galP* expression was denoted as YQ1-ctrl. Growth assays were conducted under continuous illumination of 2000–3000 lx at 30 °C and cell growth was recorded at OD_{730} every 48 h [15]. Strains WT, YQ1-ctrl and YQ2-gal showed similar growth profiles with a growth rate of 0.28/day based on OD_{730} in BG-11 medium without glucose (Fig. 1C). In the presence of 5 g/L glucose, the growth of WT and YQ1-ctrl were not affected, while growth rate showed a significant increase in YQ2-gal with efficient utilization of glucose (Fig. 1C and Additional file 1: Fig. S1A), reaching to about 5.97 times as much as WT and YQ1-ctrl.

To efficiently utilize xylose in *S. elongatus*, *xylEAB* operon from *E. coli* encoding xylose transporter, xylose isomerase and xylulokinase was integrated into *S. elongatus* chromosome at neutral site I (NSI), resulting in strain YQ3-xyl (Fig. 1D and E) [9]. Growth profiles of WT, YQ1-ctrl and YQ3-xyl were obtained under cultivation with continuous illumination of 2000–3000 lx and recorded every 48 h. Similar growth rate of 0.32/day was detected in WT, YQ1-ctrl and YQ3-xyl in BG-11 medium without xylose, while with supplementation of 5 g/L xylose, WT and YQ1-ctrl grew at a rate of 0.12/day, which is lower than that in photoautotrophic condition (Fig. 1F). Previous research has suggested that an endogenous xylose uptake system existed in wild-type cyanobacteria, while missed xylose isomerase and xylulokinase for converting xylose to central metabolites may cause metabolic imbalance [9, 10, 16], which results in a growth defect in *S. elongatus*. However, growth defect was not detected

Tan *et al. Microbial Cell Factories*   (2022) 21:31

Page 3 of 14

Fig. 1 Introduction of glucose transporter or xylose degradation pathway to *S. elongatus*. Synthetic glucose transport in *S. elongatus* (**A**). Schematic representation of glucose transporter gene *galP* into *S. elongatus* genome (**B**) and growth profile of WT (empty circle), YQ1-ctrl (gray circle) and YQ2-gal (blue circle) with and without 5 g/L glucose in BG-11 medium (**C**). Synthetic xylose degradation pathway in *S. elongatus* (**D**). Schematic representation of xylose degradation pathway into *S. elongatus* genome (**E**) and growth profile of WT (empty circle), YQ1-ctrl (gray circle) and YQ3-xyl (orange circle) with and without 5 g/L xylose in BG-11 medium (**F**). Growth assays were conducted in duplicate and error bars denoted the standard deviation from the means of independent experiments. Glu, glucose; Xyl, xylose; Xylu, xylulose; Xylu-5-P, xylulose-5-phosphate; PPP, pentose phosphate pathway; NSI, neutral site I
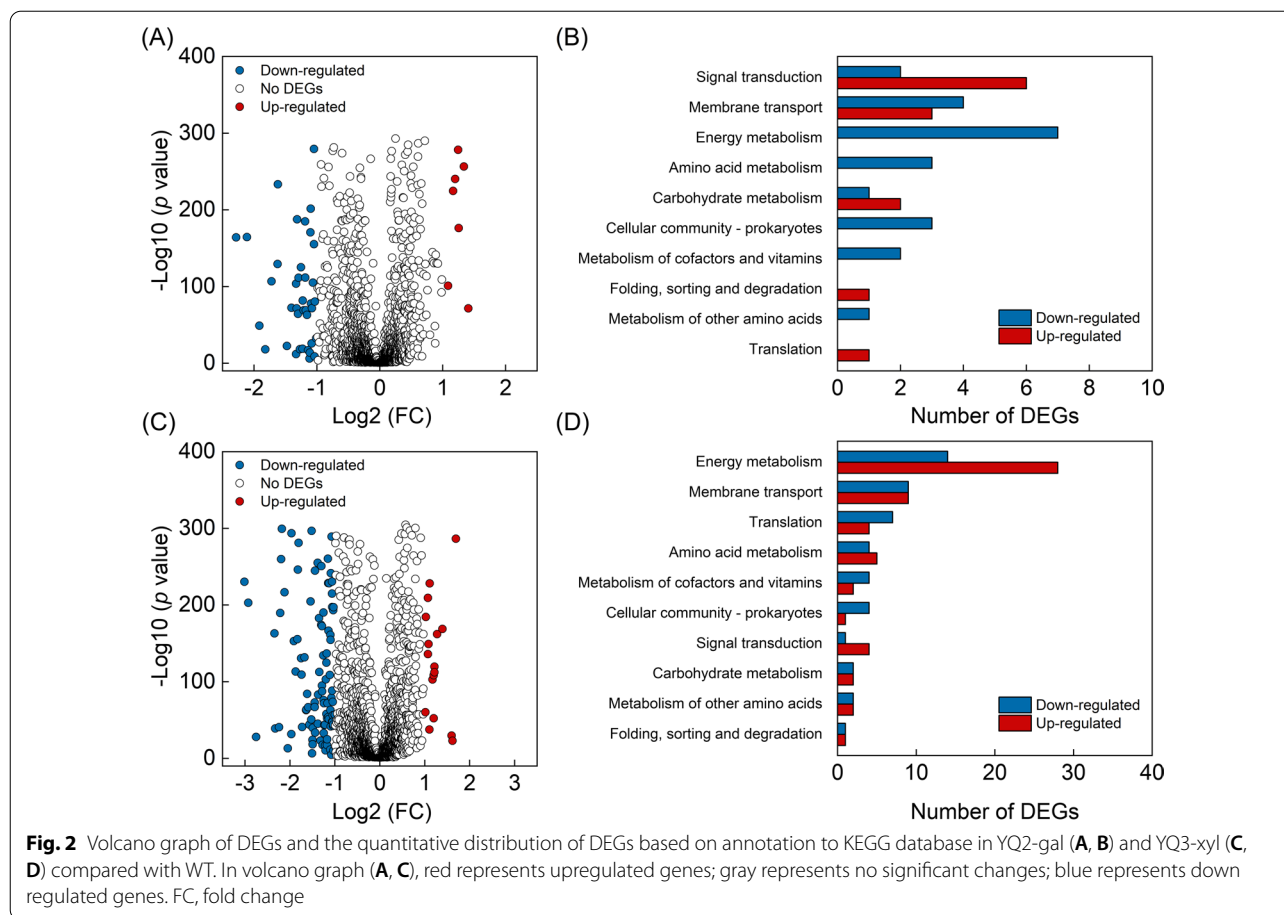
in YQ3-xyl with a complete xylose degradation pathway. This was consistent with xylose uptake profiles in Additional file 1: Fig. S1B that xylose slightly changed in WT and YQ1-ctrl, while showed significant decrease in YQ3-xyl. In the presence of xylose, YQ3-xyl even grew faster and the growth rate was 1.22 times over WT and YQ1-ctrl without xylose and 3.27 times over WT and YQ1-ctrl with the addition of xylose throughout the entire testing period of 14 days (Fig. 1F). YQ2-gal and YQ3-xyl grew well with corresponded sugar, suggesting sugar degradation pathway was successfully installed.

Overview of transcriptomics and metabolomics during photomixotrophic growth

Synthetic *S. elongatus* with efficient sugar utilization is a promising candidate for photomixotrophic study and always compared with photoautotrophic wild type for biomass and chemical production [9, 13, 14, 17]. A better understanding of metabolic alteration of engineered photomixotrophic *S. elongatus* from WT would provide insights for a more efficient and controllable photomixotrophic system. Therefore, transcriptomic and metabolomic analysis were performed in YQ2-gal and YQ3-xyl.

Transcriptome and metabolome of WT during photoautotrophic growth were set as baselines. Strains for analysis were collected at exponential phase when significant difference of growth and sugar uptake could be detected (Fig. 1 and Additional file 1: Fig. S1). Specifically, YQ2-gal was cultivated with glucose for 8 days before collection and YQ3-xyl was cultivated with xylose for 10 days before collection when YQ3-xyl significantly consumed xylose. WT was collected under the same cultivation condition but without sugar. Through the principal component analysis (PCA) of transcriptomes and metabolomes, distinct clusters of genes and metabolites were detected in YQ2-gal or YQ3-xyl and WT (Additional file 1: Figs. S2 and S3).

We found 96 DEGs with Log2 of fold change (FC) ≥ 1 or ≤ -1 and p value < 0.001 in YQ2-gal (Fig. 2A), where the regulated genes were mostly annotated as hypothetical and other functional proteins with no assignment to KEGG orthology database (Additional file 2). Other DEGs were mainly related with signal transduction (8.3%) and membrane transport (7.3%) (Fig. 2B) [18]. Among 273 DEGs with Log2 (FC) ≥ 1 or ≤ -1 and p value < 0.001 in YQ3-xyl (Fig. 2C), the largest categories

Tan *et al. Microbial Cell Factories*   (2022) 21:31

Page 4 of 14

Fig. 2 Volcano graph of DEGs and the quantitative distribution of DEGs based on annotation to KEGG database in YQ2-gal (**A**, **B**) and YQ3-xyl (**C**, **D**) compared with WT. In volcano graph (**A**, **C**), red represents upregulated genes; gray represents no significant changes; blue represents down regulated genes. FC, fold change
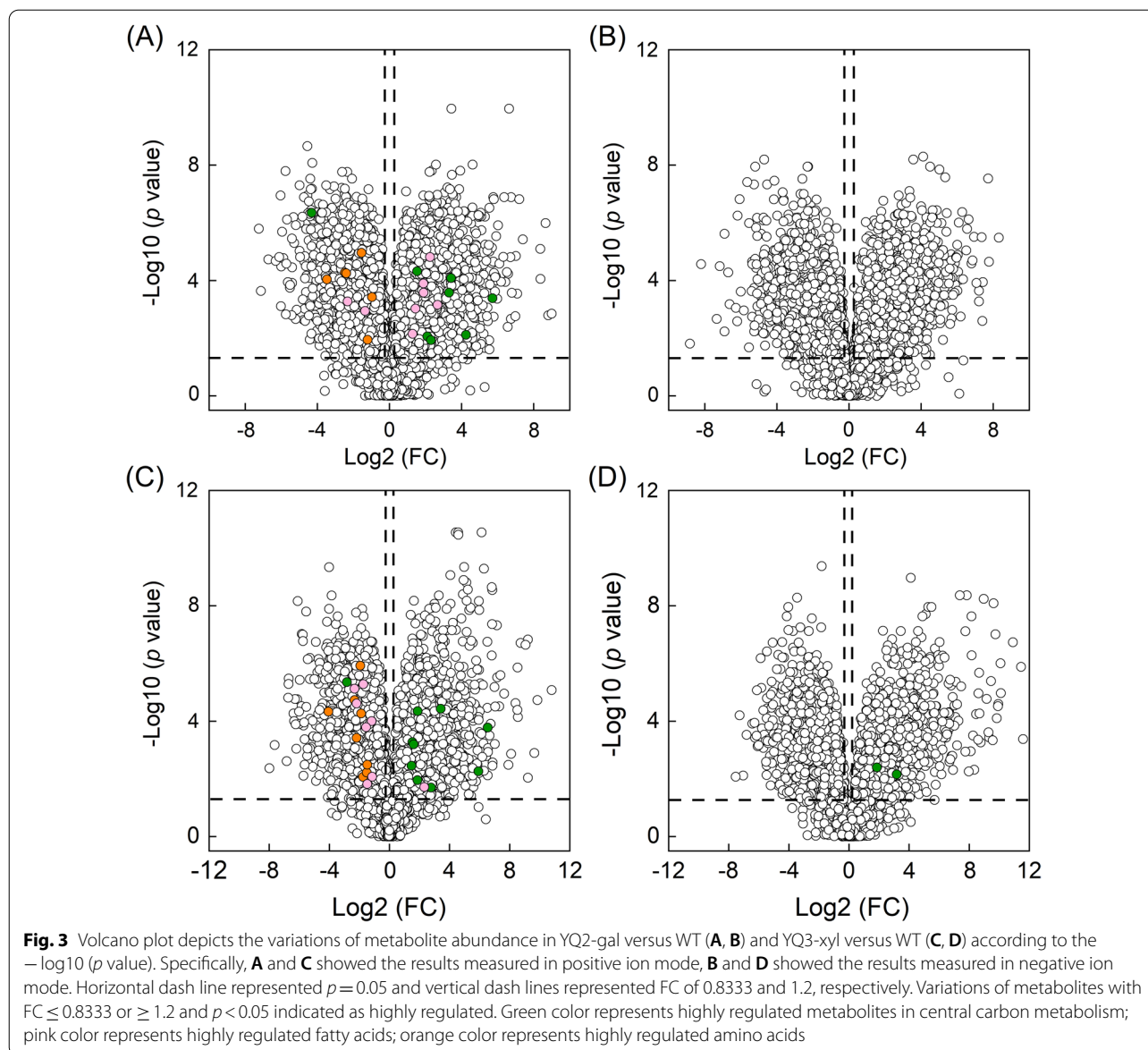
referred to KEGG orthology database are hypothetical and other functions, energy metabolism and membrane transport, comprising 41.4%, 26.7%, 15.4% and 6.6% of the total quantity of DEGs, respectively (Fig. 2D and Additional file 3) [18].

To investigate the changes of metabolites driving by sugar utilization, differential metabolites identified with FC ≥ 1.2 or ≤ 0.833 and p value < 0.05 were analyzed. Since sugar was mainly metabolized via glycolysis, pentose phosphate pathway and tricarboxylic acid (TCA) cycle, we first focused on metabolites in those pathways (Fig. 3). Metabolites in Calvin cycle were then investigated as they are the major participants for CO_2 fixation in cyanobacteria (Fig. 3). Other compounds, such as fatty acids, amino acids, sucrose and amino sugar, were also analyzed. They are produced from metabolites in carbon metabolic pathways and are important precursors for chemical production in *S. elongatus*. Variations of their abundance will help understand distribution of carbon flux and provide insights into chemical production in engineered *S. elongatus* under photomixotrophic condition (Fig. 3).

Regulations of central metabolism in engineered *S. elongatus* during photomixotrophic growth with glucose

Glycolysis is a primary pathway for glucose metabolism in microorganisms and could be affected in YQ2-gal while utilizing glucose [19, 20]. Genes in glycolysis were not differentially expressed in YQ2-gal compared with WT, while increased abundances of phosphorylated metabolites in glycolysis, such as glucose 6-phosphate (G-6-P), fructose 6-phosphate (F-6-P) and fructose 1,6-bisphosphate (F-1, 6-BP), were detected (Fig. 4). Phosphate could affect phosphorylation in glycolysis by generating ATP, thus providing energy [21, 22]. In YQ2-gal, increased phosphate with FC of 15.61 with p value < 0.05 was detected, which could provide sufficient substrate for ATP formation to meet requirement for increased phosphorylation in glycolysis. Moreover, genes in phosphate transport system were upregulated (Fig. 4). Specifically, *pstS* (Synpcc7942_2444) and *sphX* (Synpcc7942_2445) encoding phosphate-binding protein and *pstA* (Synpcc7942_2442) encoding permease protein in phosphate transport system were upregulated

Fig. 3 Volcano plot depicts the variations of metabolite abundance in YQ2-gal versus WT (**A**, **B**) and YQ3-xyl versus WT (**C**, **D**) according to the − log10 (*p* value). Specifically, **A** and **C** showed the results measured in positive ion mode, **B** and **D** showed the results measured in negative ion mode. Horizontal dash line represented *p* = 0.05 and vertical dash lines represented FC of 0.8333 and 1.2, respectively. Variations of metabolites with FC ≤ 0.8333 or ≥ 1.2 and *p* < 0.05 indicated as highly regulated. Green color represents highly regulated metabolites in central carbon metabolism; pink color represents highly regulated fatty acids; orange color represents highly regulated amino acids

with Log2 (FC) of 1.83, 3.60 and 1.03, respectively, and *p* value < 0.001. *sphR* (Synpcc7942_1012) with Log2 (FC) of 1.25 and *p* value < 0.001 may indicate higher expression of phosphate regulon response regulator, which regulates phosphate-binding protein [23, 24]. Upregulated phosphate transport system and phosphate-responsive response regulator suggested that more phosphate would be transported and provided to meet increased ATP demand in phosphorylation, which was consistent with increased phosphate in YQ2-gal [25]. No changes were detected in the downstream of glycolysis, where extra ATP is generated, suggesting similar amount of ATP was obtained in YQ2-gal and WT [26]. Even though glucose

was utilized in YQ2-gal, redundant ATP was not generated due to increased phosphorylation in glycolysis.

Pentose phosphate pathway is another major pathway for carbon metabolism [27], while most genes and metabolites involved in pentose phosphate pathway were not regulated in YQ2-gal compared with WT (Fig. 4). More upregulated metabolites in glycolysis and less changes in pentose phosphate pathway suggested that glucose was mainly degraded via glycolysis instead of pentose phosphate pathway in YQ2-gal.

TCA cycle as an important aerobic pathway for oxidation of carbohydrates starts with metabolite derived from glycolysis and pyruvate oxidation [28]. In YQ2-gal,
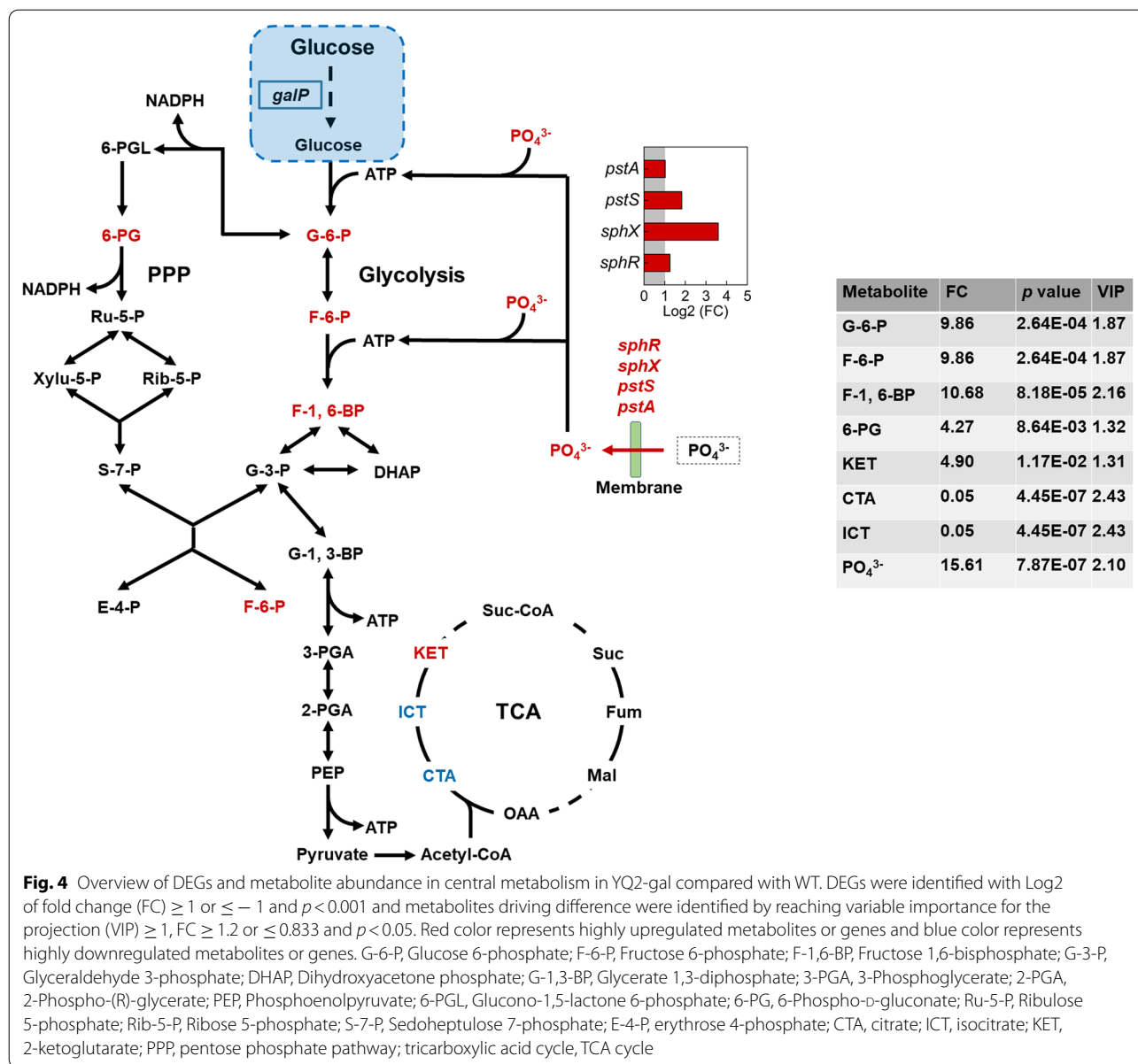
Tan *et al. Microbial Cell Factories*   (2022) 21:31

Page 6 of 14

Fig. 4 Overview of DEGs and metabolite abundance in central metabolism in YQ2-gal compared with WT. DEGs were identified with Log2 of fold change (FC) ≥ 1 or ≤ -1 and $p < 0.001$ and metabolites driving difference were identified by reaching variable importance for the projection (VIP) ≥ 1, FC ≥ 1.2 or ≤ 0.833 and $p < 0.05$. Red color represents highly upregulated metabolites or genes and blue color represents highly downregulated metabolites or genes. G-6-P, Glucose 6-phosphate; F-6-P, Fructose 6-phosphate; F-1,6-BP, Fructose 1,6-bisphosphate; G-3-P, Glyceraldehyde 3-phosphate; DHAP, Dihydroxyacetone phosphate; G-1,3-BP, Glycerate 1,3-diphosphate; 3-PGA, 3-Phosphoglycerate; 2-PGA, 2-Phospho-(R)-glycerate; PEP, Phosphoenolpyruvate; 6-PGL, Glucono-1,5-lactone 6-phosphate; 6-PG, 6-Phospho-D-gluconate; Ru-5-P, Ribulose 5-phosphate; Rib-5-P, Ribose 5-phosphate; S-7-P, Sedoheptulose 7-phosphate; E-4-P, erythrose 4-phosphate; CTA, citrate; ICT, isocitrate; KET, 2-ketoglutarate; PPP, pentose phosphate pathway; tricarboxylic acid cycle, TCA cycle

decreased citrate (CTA) and isocitrate (ICT) and increased 2-ketoglutarate (KET) were detected (Fig. 4). Glucose utilization might promote reaction from CTA and ICT to KET, thus accumulating KET in YQ2-gal.

Xylose-responsive pentose phosphate pathway and photosynthesis in engineered *S. elongatus* during photomixotrophic growth

Metabolites obtained from xylose degradation are important precursors in pentose phosphate pathway. When xylose was efficiently utilized in YQ3-xyl, metabolites in pentose phosphate pathway, such as xylulose-5-phosphate (Xylu-5-P), were increased with FC of 3.64 and

p value < 0.05 (Fig. 5). Other carbon metabolism, such as TCA cycle, showed similar results as that in YQ2-gal when compared with WT. Efficient utilization of xylose decreased CTA and ICT abundance and accumulated more KET in YQ3-xyl (Fig. 5). Genes, especially those correlated with regulated metabolites, were not differentially expressed, while genes in phosphate transport system were significantly upregulated with p value < 0.001. Specifically, genes *pstS*, *sphX*, *pstA* and *pstB* (Synpcc7942_2441) encoding ATP-binding protein were upregulated in YQ3-xyl with Log2 (FC) of 1.49, 2.60, 1.07 and 1.21, respectively (Fig. 5 and Additional file 3). More phosphate could be transported via the improved
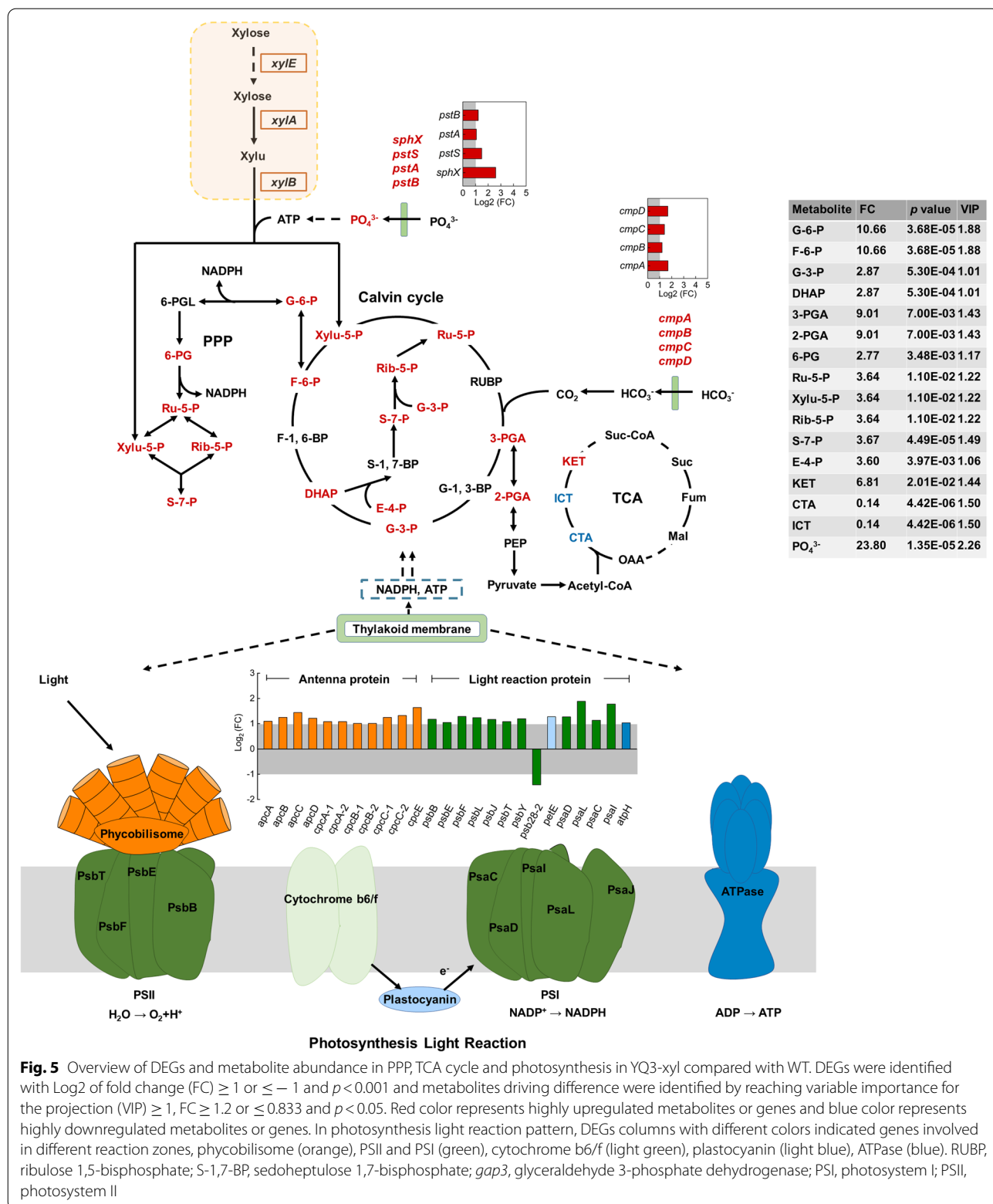
Fig. 5 Overview of DEGs and metabolite abundance in PPP, TCA cycle and photosynthesis in YQ3-xyl compared with WT. DEGs were identified with Log2 of fold change (FC) ≥ 1 or ≤ -1 and $p < 0.001$ and metabolites driving difference were identified by reaching variable importance for the projection (VIP) ≥ 1, FC ≥ 1.2 or ≤ 0.833 and $p < 0.05$. Red color represents highly upregulated metabolites or genes and blue color represents highly downregulated metabolites or genes. In photosynthesis light reaction pattern, DEGs columns with different colors indicated genes involved in different reaction zones, phycobilisome (orange), PSII and PSI (green), cytochrome b6/f (light green), plastocyanin (light blue), ATPase (blue). RUBP, ribulose 1,5-bisphosphate; S-1,7-BP, sedoheptulose 1,7-bisphosphate; *gap3*, glyceraldehyde 3-phosphate dehydrogenase; PSI, photosystem I; PSII, photosystem II

Tan *et al. Microbial Cell Factories*   (2022) 21:31

Page 8 of 14

phosphate transport system, thus providing substrates for ATP formation to generate more phosphorylated metabolites. This is in consistence with increased phosphate (with a FC of 23.80 and p value < 0.05) and phosphorylated metabolites (e.g., ribulose-5-phosphate and ribose-5-phosphate) in pentose phosphate pathway detected in YQ3-xyl via metabolome data (Fig. 5). Moreover, these upregulated metabolites in pentose phosphate pathway are also substrates for Calvin cycle in photosynthesis, where energy is needed to drive the reaction [27, 29]. Photosynthesis light reaction is a major process for energy generation in the wild-type *S. elongatus* [11], while pentose phosphate pathway is also an energy source [27]. Regulated pentose phosphate pathway may affect the photosynthesis in YQ3-xyl.

When exploring the expression level of genes in photosynthesis light reaction, most genes were significantly upregulated in YQ3-xyl (Fig. 5). Specifically, 11 out of 16 genes encoding antenna proteins for efficient harvesting of light showed upregulation (Fig. 5). Most genes in photosystem II (PSII), plastocyanin, photosystem I (PSI) and ATPase, where light is converted into NADPH and ATP, were significantly upregulated with Log2 (FC) ≥ 1 and p value < 0.001 as well (Fig. 5). Chlorophyll *a*, carotenoid and their ratio (carotenoid/chlorophyll *a*) are sensitive indicators of photosynthetic activity [30]. Specifically, chlorophyll *a* serving as major roles in both light harvesting and energy conversion showed decreased yield in YQ3-xyl compared with WT (Additional file 1: Fig. S4A) [31], indicating the reduced dependency on light for energy metabolism while extra energy source, such as pentose phosphate pathway, was provided due to xylose utilization in YQ3-xyl [32]. The yield of carotenoid had no significant change, however, carotenoid/chlorophyll *a*, which relates to the deployment of photoprotective mechanism [30, 33], were increased in YQ3-xyl (Additional file 1: Fig. S4B). Previous research has reported that energy imbalance in photosynthetic apparatus in cyanobacteria could be alleviated by photoprotective mechanisms, such as heterologous ATP-consuming pathway, to assist photosynthetic performance [34, 35]. In YQ3-xyl, even though genes in photosynthesis light reaction were significantly upregulated, energy balance could be maintained by photoprotective mechanism from ATP-consuming xylose degradation, which could be confirmed by the increase of carotenoid/chlorophyll *a*, and improved photosynthesis could be demonstrated by increased abundances of most metabolites in Calvin cycle (Fig. 5).

CO_2 is a critical participant in Calvin cycle in photosynthesis and could be obtained from bicarbonate (HCO_3^-) catalyzed by carbonic anhydrase. In YQ3-xyl, *ccaA*, *ecaA* and *ccmM* encoding carbonic anhydrase did not show particular changes. Genes *cmpABCD* (Synpcc7942_1488-1491) encoding proteins in bicarbonate transport were significantly upregulated with Log2 (FC) of 1.69, 1.20, 1.40 and 1.67, respectively, and p value < 0.001 (Fig. 5) [36, 37]. More bicarbonate may be transported into the cell by improved bicarbonate transport system with upregulated genes, thus providing more substrates for Calvin cycle in photosynthesis.

Regulated metabolisms of sucrose, glucosamine, fatty acids and amino acids in engineered *S. elongatus* in response to diverse sugar utilization

Metabolites from glycolysis, pentose phosphate pathway, TCA cycle and Calvin cycle are important precursors for sucrose, glucosamine, fatty acids and amino acids. With utilization of glucose or xylose, regulated precursors may affect biosynthesis of these metabolites. For instance, increased G-1-P and F-6-P by efficient utilization of glucose may be a main reason for a 1.89-fold and 17.88-fold increase of sucrose and glucosamine (GlcN) in YQ2-gal when compared with that in WT (Fig. 6). Moreover, significant increase of GlcN with p value < 0.05 indicated that more carbon flowed into GlcN biosynthesis in YQ2-gal during photomixotrophic growth with glucose. Fatty acids are produced from acetyl-CoA [3]. Most fatty acids, especially long-chain fatty acids with more than 20 carbons, were increased in YQ2-gal (Fig. 6). Another metabolite of acetyl-CoA, acetaldehyde, was also increased with a fold change of 52.45 (p value < 0.05) when compared with WT (Fig. 6). Even though significant change was not detected in acetyl-CoA, increased fatty acids and acetaldehyde indicated the increased carbon flux through acetyl-CoA. With more carbon flowed into sugar and fatty acids biosynthesis, amino acids biosynthesis may be affected. In YQ2-gal, seven out of 15 amino acids had decreased abundance when compared with that in WT (Fig. 6). Moreover, genes in branched-chain amino acid transport were downregulated in YQ2-gal (Fig. 6). Genes *natD* (Synpcc7942_2495) and *livM* (Synpcc7942_2494) encoding permease and *natA* (Synpcc7942_2493) encoding ATP-binding protein in amino acid transport showed downregulation with Log2 (FC) of -1.31, -1.39 and -1.31, respectively, and p value < 0.001 in YQ2-gal compared with WT. Amino acid transport is bidirectional and could be regulated by corresponding genes [38]. Downregulated genes would mitigate branched-chain amino acid transport, thus maintaining intracellular amino acid level (leucine, isoleucine and threonine) in YQ2-gal.

Similar results of increased sucrose with a FC of 3.05 (p value < 0.05) and GlcN with a FC of 60.27 (p value < 0.05) were also detected in YQ3-xyl (Fig. 7). However, most fatty acids were decreased in YQ3-xyl (Fig. 7). More sugars and acetaldehyde (92.48-fold with p value < 0.05)
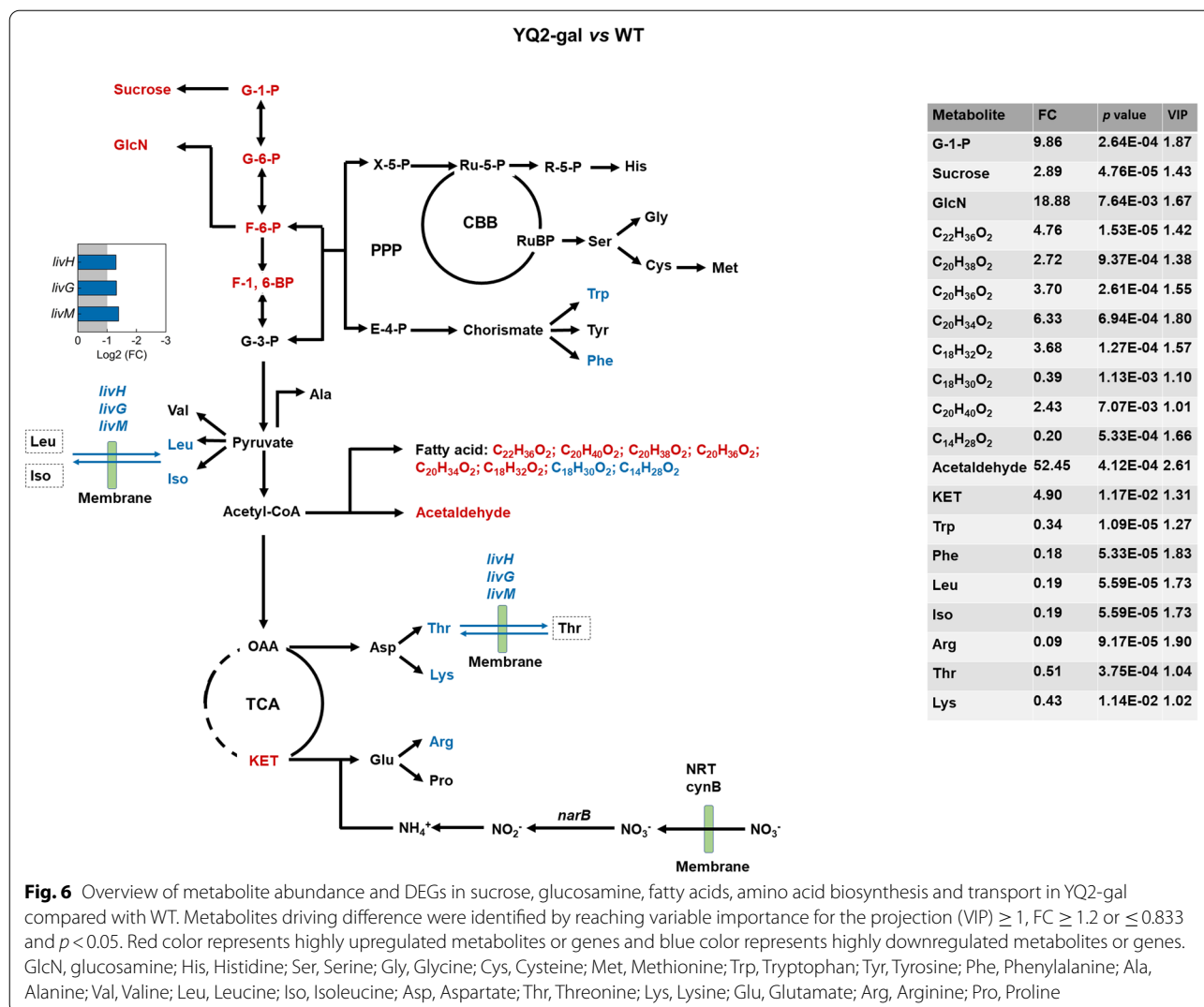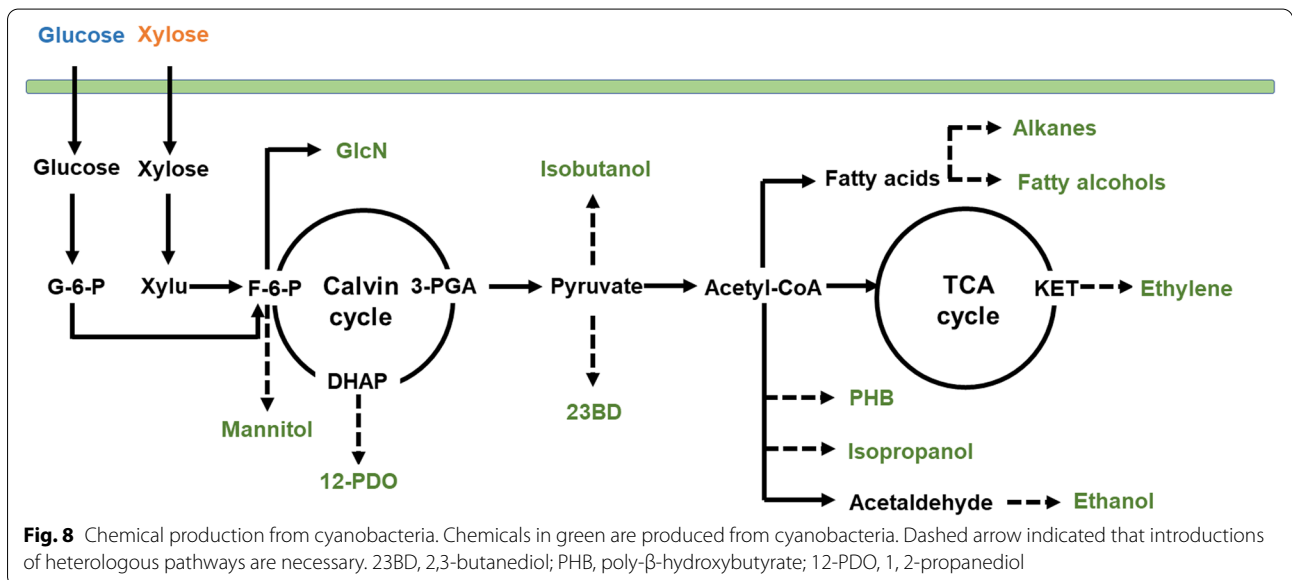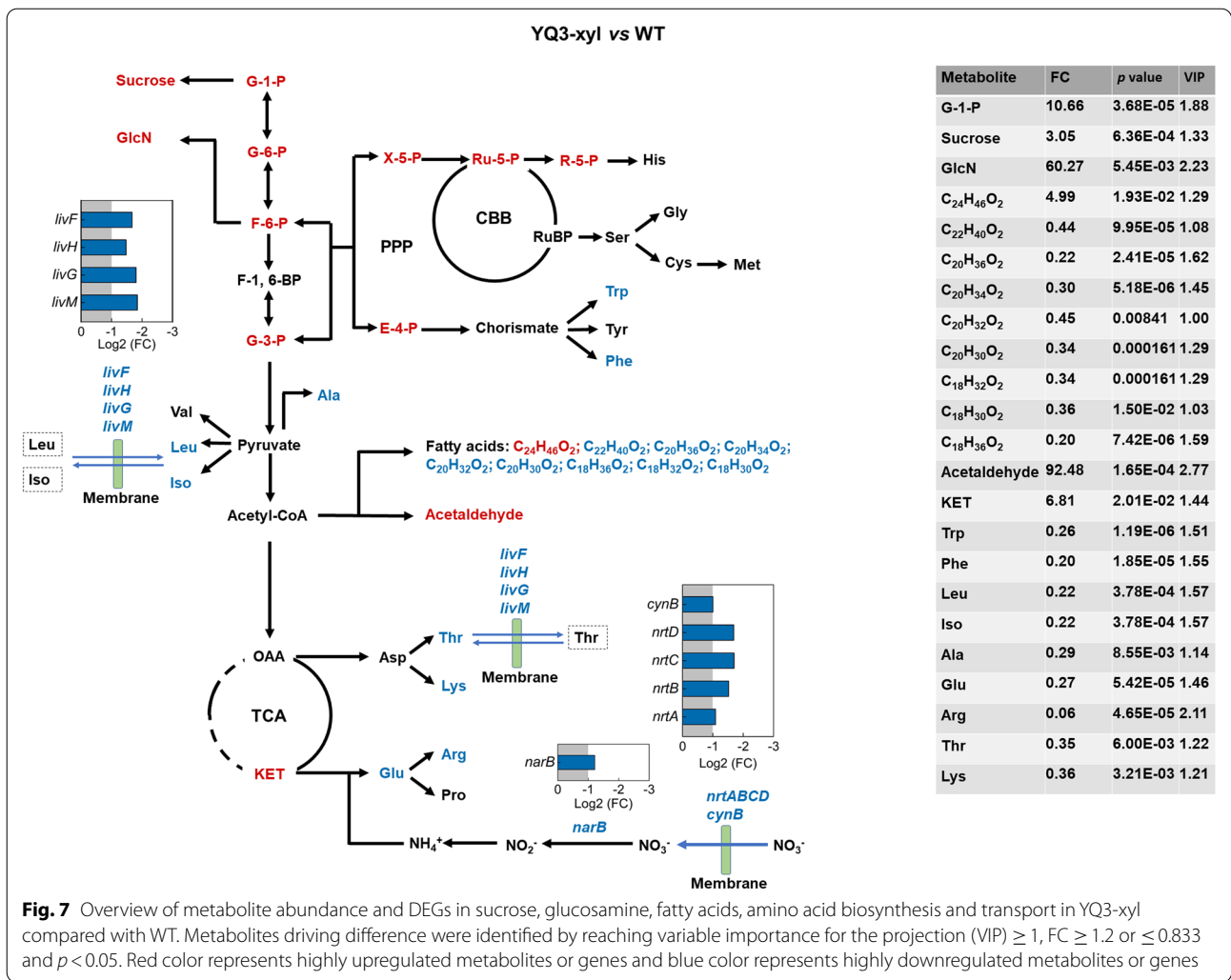
Tan *et al. Microbial Cell Factories*   (2022) 21:31

Page 9 of 14

Fig. 6 Overview of metabolite abundance and DEGs in sucrose, glucosamine, fatty acids, amino acid biosynthesis and transport in YQ2-gal compared with WT. Metabolites driving difference were identified by reaching variable importance for the projection (VIP) ≥ 1, FC ≥ 1.2 or ≤ 0.833 and $p < 0.05$. Red color represents highly upregulated metabolites or genes and blue color represents highly downregulated metabolites or genes. GlcN, glucosamine; His, Histidine; Ser, Serine; Gly, Glycine; Cys, Cysteine; Met, Methionine; Trp, Tryptophan; Tyr, Tyrosine; Phe, Phenylalanine; Ala, Alanine; Val, Valine; Leu, Leucine; Iso, Isoleucine; Asp, Aspartate; Thr, Threonine; Lys, Lysine; Glu, Glutamate; Arg, Arginine; Pro, Proline

production indicated that carbon was redistributed with less into fatty acids biosynthesis in YQ3-xyl. In amino acids metabolism, decreased amino acid and downregulated gene expression in amino acid transport were also detected in YQ3-xyl when compared with WT (Fig. 7). In addition, genes in nitrate (NO_3^-) transport and assimilation were downregulated. In *Synechococcus*, extracellular nitrate is first transferred into cells by passive diffusion or by active transport mediated via ABC-type transporters encoded by *nrtA*(Synpcc7942_1239), *nrtB* (Synpcc7942_1238), *nrtC* (Synpcc7942_1237) and *nrtD* (Synpcc7942_1236), then nitrate could be reduced to nitrite (NO_2^-) catalyzed by nitrate reductase encoded by *narB* (Synpcc7942_1235) and further reduced to ammonia (NH_4^+), which is a major substrate for amino acid biosynthesis, especially for glutamate biosynthesis. In YQ3-xyl, *nrtABCD* were downregulated with Log2 (FC) ≤ − 1 and p value < 0.001 (Fig. 7). Gene *cynB*

(Synpcc7942_2106) encoding ABC-type cyanate transporter which could transport nitrate, showed downregulation as well [39]. *narB* in YQ3-xyl was negatively expressed with Log2 (FC) of − 1.21 and $p < 0.001$. Downregulation of genes in nitrate transport and assimilation to nitrite may affect ammonia production, thus impacting on glutamate biosynthesis (Fig. 7). This is consistent with decreased abundance of glutamate in YQ3-xyl.

Perspectives for photomixotrophic bioproduction in cyanobacteria

Cyanobacteria have been engineered to produce a wide range of chemicals, and synthetic photomixotrophic strains have been applied as chassis to further increase the productivity using additional carbon sources (Fig. 8) [13, 40]. For instance, the productivity of 23BD and isobutanol could be significantly increased in cyanobacteria with utilization of glucose or xylose [14, 17]. In the

Tan *et al. Microbial Cell Factories*   (2022) 21:31

Page 10 of 14

Fig. 7 Overview of metabolite abundance and DEGs in sucrose, glucosamine, fatty acids, amino acid biosynthesis and transport in YQ3-xyl compared with WT. Metabolites driving difference were identified by reaching variable importance for the projection (VIP) ≥ 1, FC ≥ 1.2 or ≤ 0.833 and $p < 0.05$. Red color represents highly upregulated metabolites or genes and blue color represents highly downregulated metabolites or genes

Metabolite	FC	p value	VIP
G-1-P	10.66	3.68E-05	1.88
Sucrose	3.05	6.36E-04	1.33
GlcN	60.27	5.45E-03	2.23
$C_{24}H_{46}O_2$	4.99	1.93E-02	1.29
$C_{22}H_{40}O_2$	0.44	9.95E-05	1.08
$C_{20}H_{36}O_2$	0.22	2.41E-05	1.62
$C_{20}H_{34}O_2$	0.30	5.18E-06	1.45
$C_{20}H_{32}O_2$	0.45	0.00841	1.00
$C_{20}H_{30}O_2$	0.34	0.000161	1.29
$C_{18}H_{32}O_2$	0.34	0.000161	1.29
$C_{18}H_{30}O_2$	0.36	1.50E-02	1.03
$C_{18}H_{36}O_2$	0.20	7.42E-06	1.59
Acetaldehyde	92.48	1.65E-04	2.77
KET	6.81	2.01E-02	1.44
Trp	0.26	1.19E-06	1.51
Phe	0.20	1.85E-05	1.55
Leu	0.22	3.78E-04	1.57
Iso	0.22	3.78E-04	1.57
Ala	0.29	8.55E-03	1.14
Glu	0.27	5.42E-05	1.46
Arg	0.06	4.65E-05	2.11
Thr	0.35	6.00E-03	1.22
Lys	0.36	3.21E-03	1.21

Fig. 8 Chemical production from cyanobacteria. Chemicals in green are produced from cyanobacteria. Dashed arrow indicated that introductions of heterologous pathways are necessary. 23BD, 2,3-butanediol; PHB, poly-β-hydroxybutyrate; 12-PDO, 1, 2-propanediol

Tan *et al. Microbial Cell Factories*   (2022) 21:31

Page 11 of 14

presence of xylose, an ethylene-producing strain with introduction of xylose degradation pathway enhanced the ethylene production [10], partially due to the increased substrate of KET.

Even though glucose or xylose has not been applied in other chemical production, increased F-6-P, DHAP and acetaldehyde indicated that production of mannitol, 1, 2-propanediol (12-PDO) and ethanol has great potentials to be increased in cyanobacteria with efficient utilization of sugars, since sufficient precursors are provided (Fig. 8) [41–44]. Other substrates (e.g., acetyl-CoA) for chemical production (e.g., isopropanol and poly-β-hydroxybutyrate, PHB) were not detected with regulations by sugar utilization (Fig. 8) [45, 46]. However, regulated metabolites (e.g., acetaldehyde) indicated the changed carbon flux through the precursors. To increase the productivity of desired chemicals, modifications of synthetic pathway, such as overexpressing related genes, and repressing genes in bypass, may be an efficient way to utilize sugars during bioproduction. Moreover, sucrose functions both as osmoprotectant and as an energy reserve in cyanobacteria [47, 48]. Increased sucrose accumulation in cyanobacteria with efficient utilization of both sugars suggested the enhanced tolerance to stress conditions and the promoted metabolism under dark condition. GlcN as a dietary supplement for joint health also showed significant increase with both sugar utilization [49], suggesting a potential drug production in synthetic photomixotrophic cyanobacteria.

However, metabolites, such as fatty acids, showed dramatically different changes in synthetic photomixotrophic cyanobacteria when compared with WT. Most fatty acids were increased in glucose-consuming strain, while decreased in xylose-consuming strain. Therefore, effect of different sugars should be considered and optimization of synthetic pathways should be conducted during photomixotrophic production of fatty alcohols and alkanes (Fig. 8) [50, 51]. Detailed information from transcriptomic and metabolic analysis of cyanobacteria during photomixotrophic growth could bring up new insights and offer valuable guidance to photomixotrophic bioproduction using this potential chassis.

Conclusions

Due to the redirected carbon flux and transcriptional perturbations, carbon metabolism, fatty acids and amino acid synthesis, and membrane transport were regulated in engineered *S. elongatus* during photomixotrophic growth with sugars, where fatty acids metabolism was differently regulated in response to glucose and xylose utilization. Moreover, regulated photosynthesis in engineered *S. elongatus* with xylose utilization indicated that light dependency could be modulated under

photomixotrophic condition. Since these metabolic regulations are closely correlated with chemical productions, we envision this study would bring some guidance for photomixotrophic bioproduction using this rising microbial chassis.

Methods

Chemicals and reagents

All the chemicals used in this study were at analytical grade and purchased from the Sinopharm Chemical Reagent company (China) unless otherwise specified. Enzymes and kits used for molecular cloning were purchased from New England Biolabs (NEB, USA). Oligonucleotides were synthesized by Beijing Genomics Institute (BGI, China). Spectinomycin and IPTG (Isopropyl-β-D-thiogalactopyranoside) used in this study were obtained from MDBio (MDBio, Inc., China) and Biotopped (Biotopped Life Science, China), respectively.

Strain, medium and growth conditions

All cyanobacterial strains used in this study were summarized in Table 1 and cultured in BG-11 media at 30 °C with continuous illumination of 2000–3000 lx [15]. Spectinomycin (20 μg/mL) and IPTG (0.1 mM) were added to select recombinant strains and induce the P_{trc} promoter. Glucose 5 g/L (27.78 mM) or xylose of 5 g/L (33.33 mM) was supplemented as organic carbon source.

All *Escherichia coli* strains were cultivated in LB medium (5 g/L of yeast extract, 10 g/L of tryptone, 10 g/L of NaCl, pH 7.0) at 37 °C. *E. coli* MG1655 genomic DNA was used as a PCR template for target gene amplification. *E. coli* DH5α was used for plasmid construction and propagation. Spectinomycin (20 μg/mL) was added for selecting transformants harboring a plasmid.

DNA manipulation, plasmid and strain construction

All primers and plasmids used in this study were listed in Additional file 1: Table S1 and S2. Genes *galP*, *xylE*, *xylA* and *xylB* were amplified from *E. coli* MG1655 genomic DNA. *galP* gene was amplified using primers G1 and G2, digested with MfeI and BglII, and then ligated with pAM2991 digested with EcoRI and BamHI to create pAM2991-*galP*. *xylE* gene was amplified by primers X1 and X2. *xylAB* genes was amplified by primers

Table 1 Cyanobacterial strains used in this study

Names	Description	Sources
WT	*S. elongatus* PCC7942 (wild type)	ATCC 33912
YQ1-ctrl	WT, P$_{Trc}$-*MCS* integrated in NSI	This study
YQ2-gal	WT, P$_{Trc}$-*galP* integrated in NSI	This study
YQ3-xyl	WT, P$_{Trc}$-*xylEAB* integrated in NSI	This study

X3 and X4. Two fragments of pAM2991 template were amplified by primers V1 and V2, V3 and V4, respectively. Gibson Assembly was applied to fuse these four gene fragments to create pAM2991-*xylEAB*. Plasmids carrying target genes or empty backbone were then transformed into *S. elongatus* following the method described previously [52]. Briefly, *S. elongatus* at exponential phase was collected and transformation was conducted at 30 °C with gentle agitation overnight in the dark. Transformants were selected by spectinomycin and correct recombinants were confirmed by colony PCR to verify integration into cyanobacterial chromosome at NSI. Cyanobacterial strains used and constructed were listed in Table 1.

Growth assays

Cyanobacterial strains collected from exponential phase were diluted to an OD_{730} of 0.2 in 50 mL BG-11 medium including spectinomycin and IPTG. Wild-type assays omitted addition of spectinomycin and IPTG. Glucose or xylose was added to provide exogenous carbon source. Cell growth was recorded at OD_{730} every 24 h using a spectrophotometer (JINGHUA Instruments, China). Sugar concentrations were measured by high-performance liquid chromatography (HPLC, Shimadzu LC-20AT) equipped with a refractive index detector and a Rezex ROA-Organic Acid H^+ (8%) column (Phenomenex Inc., Torrance, CA). The column was eluted with 0.005 N of H_2SO_4 at a flow rate of 0.6 mL/min at 50 °C.

Pigment quantification

Chlorophyll *a* and carotenoids were measured based on a method reported previously [53]. Briefly, chlorophyll *a* and carotenoids were extracted by re-suspending the cell pellet (1 mL cell culture, centrifuged at 15,000*g* for 7 min) in 100% methanol at 4 °C for 20 min. The extract absorbance was measured at 470 nm, 665 nm and 720 nm, and concentrations of pigments were calculated according to the equations [54, 55]:

$$\text{Chlorophyll } a \, (\mu g/mL) = 12.9447(A665 - A720)$$

$$\text{Carotenoid } (\mu g/mL) = (1000 \, (A470 - A720) - 2.86 \, (\text{Chlorophyll } a \, (\mu g/mL)))/221$$

RNA sequencing

Cells at exponential phase with three biological replicates were collected and submitted to BGI for RNA sequencing. Total RNA was isolated and purified at BGI with quality and concentration determined by Bioanalyzer 2100 (Agilent). Library construction and RNA sequencing were performed on BGISEQ-500 platform (BGI,

China) using Combinational Probe-Anchor Synthesis Sequencing Method. All raw sequencing reads were trimmed based on adaptors, reads where unknown bases reached more than 10%, and low quality. Clean reads were then obtained and mapped to genome of *S. elongatus* by HISAT [56]. Gene expression level was quantified by RSEM and normalization procedures was processed with FPKM [57, 58]. DEGseq method was used to screen differentially expressed genes with Log2 (FC) ≥ 1 or ≤ -1 and p value < 0.001 [59].

Metabolomics profiling

Strains with six biological replicates were collected at exponential phase for metabolomics profiling. Metabolites were extracted as previously described [60]. Briefly, 300 μL cold methanol was added into 100 μL sample and cells were broken using TissueLyser at 50 Hz for 4 min. After standing for 2 h in -20 °C, all samples were centrifuged at 30,000*g*, 4 °C for 20 min. Supernatants were collected for each sample. A quality control (QC) sample was made by mixing 35 μL from each sample supernatant to estimate a mean profile representing all the analytes encountered during analysis. All supernatants as well as QC sample were subjected to metabolomics profiling by 2777C UPLC system (Water, UK) coupled with mass spectrometer Xevo G2-XS QTOF (Waters, UK) in BGI. Both positive and negative mode were operated. To evaluate the stability of LC–MS during the whole acquisition, a QC sample was acquired after every 10 samples. Raw data were imported into Progenesis QI software and then preprocessed using metaX software. Features detected in less than 50% of the QC samples or less than 20% of the experimental samples were removed, and missing values were imputed using the k-nearest neighbor (KNN) method. The QC-robust spline batch correction (QC-RSC) was used to correct signal drift and batch variation. The relative s.d. (RSD) value of metabolites in the QC samples was set at a threshold of 30%, and features with a RSD less than 30% in the QC samples were retained [60]. After normalization and filtering, univariate and multivariate were conducted by metaX. To identify metabolites, standards were used and molecular mass data were matched to KEGG and BGI own database Met-Lib for a further check. Metabolites driving differences were identified by reaching variable importance for the projection (VIP) ≥ 1, FC ≥ 1.2 or ≤ 0.833 and p value < 0.05.

Tan *et al. Microbial Cell Factories*   (2022) 21:31

Page 13 of 14

Abbreviations

CO_2: Carbon dioxide; RuBisCO: Ribulose-1,5-bisphosphate carboxylase/oxygenase; DEGs: Differentially expressed genes; FC: Fold change; NSI: Neutral site I; PPP: Pentose phosphate pathway; TCA cycle: Tricarboxylic acid cycle; Glu: Glucose; Xyl: Xylose; Xylu: Xylulose; Xylu-5-P: Xylulose-5-phosphate; G-6-P: Glucose 6-phosphate; F-6-P: Fructose 6-phosphate; F-1,6-BP: Fructose 1,6-bisphosphate; G-3-P: Glyceraldehyde 3-phosphate; DHAP: Dihydroxyacetone phosphate; G-1,3-BP: Glycerate 1,3-diphosphate; 3-PGA: 3-Phosphoglycerate; 2-PGA: 2-Phospho-(R)-glycerate; PEP: Phosphoenolpyruvate; CTA: Citrate; ICT: Isocitrate; KET: 2-Ketoglutarate; 6-PGL: Glucono-1,5-lactone 6-phosphate; 6-PG: 6-Phospho-D-gluconate; Ru-5-P: Ribulose 5-phosphate; Rib-5-P: Ribose 5-phosphate; S-7-P: Sedoheptulose 7-phosphate; E-4-P: Erythrose 4-phosphate; RUBP: Ribulose 1,5-bisphosphate; S-1,7-BP: Sedoheptulose 1,7-bisphosphate; *gap3*: Glyceraldehyde 3-phosphate dehydrogenase; PSI: Photosystem I; PSII: Photosystem II; GlcN: Glucosamine; His: Histidine; Ser: Serine; Gly: Glycine; Cys: Cysteine; Met: Methionine; Trp: Tryptophan; Tyr: Tyrosine; Phe: Phenylalanine; Ala: Alanine; Val: Valine; Leu: Leucine; Iso: Isoleucine; Asp: Aspartate; Thr: Threonine; Lys: Lysine; Glu: Glutamate; Arg: Arginine; Pro: Proline; 23BD: 2,3-Butanediol; PHB: Poly-β-hydroxybutyrate; IPTG: Isopropyl-β-D-thiogalactopyranoside; VIP: Variable importance for the projection.

Supplementary Information

The online version contains supplementary material available at https://doi.org/10.1186/s12934-022-01760-1.

Additional file 1: Fig. S1 Sugar consumption profiles of WT (empty circle), YQ1-ctrl (gray circle) and YQ2-gal (blue circle) in BG-11 medium with 5 g/L glucose (A) and WT (empty circle), YQ1-ctrl (gray circle) and YQ3-xyl (orange circle) in BG-11 medium with 5 g/L xylose (B). Error bars represent standard deviations (in duplicate). **Fig. S2** Principal component analysis (PCA) of transcriptomics data for replicates of YQ2-gal and WT (A) and YQ3-xyl and WT (B). **Fig. S3** Principal component analysis (PCA) of metabolomics data for replicates of YQ2-gal and WT (A, B), and YQ3-xyl and WT (C, D). Specifically, A and C represents the results in positive ion mode, B and D represents the results in negative ion mode. **Fig. S4** Pigment measurement (A) and carotenoid/chlorophyll *a* (B) of WT (white) during photoautotrophic growth and YQ3-xyl (orange) during photomixotrophic growth. Error bars represent standard deviations (in triplicate). * represents significant difference with *p* value less than 0.05, ** represents significant difference with *p* value less than 0.01. **Table S1** Primers used in this study. **Table S2** Plasmids used in this study.

Additional file 2. DEGs in YQ2-gal strain during photomixotrophic growth with glucose.

Additional file 3. DEGs in YQ3-xyl strain during photomixotrophic growth with xylose.

Author details
[1]Shandong Key Laboratory of Water Pollution Control and Resource Reuse, School of Environmental Science and Engineering, Shandong University, Qingdao 266237, China. [2]Sino-French Research Institute for Ecology and Environment (ISFREE), Shandong University, Qingdao 266237, China.

References

1. Luan G, Lu X. Tailoring cyanobacterial cell factory for improved industrial properties. Biotechnol Adv. 2018;36:430–42.
2. Lin P-C, Zhang F, Pakrasi HB. Enhanced limonene production in a fast-growing cyanobacterium through combinatorial metabolic engineering. Metab Eng Commu. 2021;12:e00164.
3. Oliver NJ, Rabinovitch-Deere CA, Carroll AL, Nozzi NE, Case AE, Atsumi S. Cyanobacterial metabolic engineering for biofuel and chemical production. Curr Opin Chem Biol. 2016;35:43–50.
4. Zhang C-C, Jeanjean R, Joset F. Obligate phototrophy in cyanobacteria: more than a lack of sugar transport. FEMS Microbiol Lett. 1998;161:285–92.
5. Kachel B, Mack M. Engineering of *Synechococcus* sp. strain PCC 7002 for the photoautotrophic production of light-sensitive riboflavin (vitamin B2). Metab Eng. 2020;62:275–86.
6. Liang F, Englund E, Lindberg P, Lindblad P. Engineered cyanobacteria with enhanced growth show increased ethanol production and higher biofuel to biomass ratio. Metab Eng. 2018;46:51–9.
7. Liang F, Lindblad P. *Synechocystis* PCC 6803 overexpressing RuBisCO grow faster with increased photosynthesis. Metab Eng Commu. 2017;4:29–36.
8. Huang F, Kong W-W, Sun Y, Chen T, Dykes GF, Jiang Y-L, Liu L-N. Rubisco accumulation factor 1 (Raf1) plays essential roles in mediating Rubisco assembly and carboxysome biogenesis. Proc Natl Acad Sci USA. 2020;117:17418.
9. McEwen JT, Machado IMP, Connor MR, Atsumi S. Engineering *Synechococcus elongatus* PCC 7942 for continuous growth under diurnal conditions. Appl Environ Microbiol. 2013;79:1668.
10. Lee T-C, Xiong W, Paddock T, Carrieri D, Chang I-F, Chiu H-F, Ungerer J, Hank Juo S-H, Maness P-C, Yu J. Engineered xylose utilization enhances bio-products productivity in the cyanobacterium *Synechocystis* sp. PCC 6803. Metab Eng. 2015;30:179–89.
11. Kanno M, Carroll AL, Atsumi S. Global metabolic rewiring for improved CO_2 fixation and chemical production in cyanobacteria. Nat Commun. 2017;8:14724.
12. Kanno M, Atsumi S. Engineering an obligate photoautotrophic cyanobacterium to utilize glycerol for growth and chemical production. ACS Synth Biol. 2017;6:69–75.

13. Matson MM, Atsumi S. Photomixotrophic chemical production in cyano-bacteria. Curr Opin Biotechnol. 2018;50:65–71.
14. McEwen JT, Kanno M, Atsumi S. 2,3 Butanediol production in an obligate photoautotrophic cyanobacterium in dark conditions via diverse sugar consumption. Metab Eng. 2016;36:28–36.
15. Cao YQ, Li Q, Xia PF, Wei LJ, Guo N, Li JW, Wang SG. AraBAD based toolkit for gene expression and metabolic robustness improvement in *Synechococcus elongatus*. Sci Rep. 2017;7:18059.
16. Jojima T, Omumasaba CA, Inui M, Yukawa H. Sugar transporters in efficient utilization of mixed sugar substrates: current knowledge and outlook. Appl Microbiol Biotechnol. 2010;85:471–80.
17. Varman AM, Xiao Y, Pakrasi HB, Tang YJ. Metabolic engineering of *Synechocystis* sp. Strain PCC 6803 for isobutanol production. Appl Environ Microbiol. 2013;79:908.
18. Rubin BE, Wetmore KM, Price MN, Diamond S, Shultzaberger RK, Lowe LC, Curtin G, Arkin AP, Deutschbauer A, Golden SS. The essential gene set of a photosynthetic organism. Proc Natl Acad Sci USA. 2015;112:E6634.
19. Bogorad IW, Lin T-S, Liao JC. Synthetic non-oxidative glycolysis enables complete carbon conservation. Nature. 2013;502:693–7.
20. Song X, Diao J, Yao J, Cui J, Sun T, Chen L, Zhang W. Engineering a central carbon metabolism pathway to increase the intracellular acetyl-CoA pool in *Synechocystis* sp. PCC 6803 grown under photomixotrophic conditions. ACS Synth Biol. 2021;10:836–46.
21. Folch PL, Bisschops MMM, Weusthuis RA. Metabolic energy conservation for fermentative product formation. Microb Biotechnol. 2021;14(3):829–58.
22. Post RL, Toda G, Rogers FN. Phosphorylation by inorganic phosphate of sodium plus potassium ion transport adenosine triphosphatase. Four reactive states. J Biol Chem. 1975;250:691–701.
23. Nagaya M, Aiba H, Mizuno T. The sphR product, a two-component system response regulator protein, regulates phosphate assimilation in *Synechococcus* sp. strain PCC 7942 by binding to two sites upstream from the phoA promoter. J Bacteriol. 1994;176:2210.
24. Boyd JS, Cheng RR, Paddock ML, Sancar C, Morcos F, Golden SS. A combined computational and genetic approach uncovers network interactions of the cyanobacterial circadian clock. J Bacteriol. 2016;198:2439.
25. Martín JF, Liras P. Molecular mechanisms of phosphate sensing, transport and signalling in *Streptomyces* and related actinobacteria. Int J Mol Sci. 2021. https://doi.org/10.3390/ijms22031129.
26. Wright B, Bishop DW. Respiration and fermentation. Science. 1962;135:444.
27. Shinde S, Zhang X, Singapuri SP, Kalra I, Liu X, Morgan-Kiss RM, Wang X. Glycogen metabolism supports photosynthesis start through the oxidative pentose phosphate pathway in cyanobacteria. Plant Physiol. 2020;182:507–17.
28. Xiong W, Cano M, Wang B, Douchi D, Yu J. The plasticity of cyanobacterial carbon metabolism. Curr Opin Chem Biol. 2017;41:12–9.
29. Levin E, Lopez-Martinez G, Fane B, Davidowitz G. Hawkmoths use nectar sugar to reduce oxidative damage from flight. Science. 2017;355:733.
30. Gitelson A. Towards a generic approach to remote non-invasive estimation of foliar carotenoid-to-chlorophyll ratio. J Plant Physiol. 2020;252:153227.
31. Björn LO, Papageorgiou GC, Blankenship RE, Govindjee. A viewpoint: why chlorophyll *a*? Photosynth Res. 2009;99:85–98.
32. Sarnaik A, Pandit R, Lali A. Growth engineering of *Synechococcus elongatus* PCC 7942 for mixotrophy under natural light conditions for improved feedstock production. Biotechnol Prog. 2017;33:1182–92.
33. Chamovitz D, Sandmann G, Hirschberg J. Molecular and biochemical characterization of herbicide-resistant mutants of cyanobacteria reveals that phytoene desaturation is a rate-limiting step in carotenoid biosynthesis. J Biol Chem. 1993;268:17348–53.
34. Kirst H, Formighieri C, Melis A. Maximizing photosynthetic efficiency and culture productivity in cyanobacteria upon minimizing the phycobilisome light-harvesting antenna size. Biochim Biophys Acta Bioenerg. 2014;1837:1653–64.
35. Santos-Merino M, Torrado A, Davis GA, Röttig A, Bibby TS, Kramer DM, Ducat DC. Improved photosynthetic capacity and photosystem I oxidation via heterologous metabolism engineering in cyanobacteria. Proc Natl Acad Sci USA. 2021;118:e2021523118.
36. Omata T, Price GD, Badger MR, Okamura M, Gohta S, Ogawa T. Identification of an ATP-binding cassette transporter involved in bicarbonate uptake in the cyanobacterium *Synechococcus* sp. strain PCC 7942. Proc Natl Acad Sci USA. 1999;96:13571.
37. Omata T, Gohta S, Takahashi Y, Harano Y, Maeda S-i. Involvement of a CbbR homolog in low CO_2-induced activation of the bicarbonate transporter operon in cyanobacteria. J Bacteriol. 2001;183:1891.
38. Hosie AHF, Poole PS. Bacterial ABC transporters of amino acids. Res Microbiol. 2001;152:259–70.
39. Maeda S-i, Omata T. Nitrite transport activity of the ABC-Type cyanate transporter of the cyanobacterium *Synechococcus elongatus*. J Bacteriol. 2009;191:3265.
40. Angermayr SA, Gorchs Rovira A, Hellingwerf KJ. Metabolic engineering of cyanobacteria for the synthesis of commodity products. Trends Biotechnol. 2015;33:352–61.
41. Jacobsen JH, Frigaard N-U. Engineering of photosynthetic mannitol biosynthesis from CO_2 in a cyanobacterium. Metab Eng. 2014;21:60–70.
42. Li H, Liao JC. Engineering a cyanobacterium as the catalyst for the photosynthetic conversion of CO_2 to 1,2-propanediol. Microb Cell Fact. 2013;12:4.
43. Luan G, Qi Y, Wang M, Li Z, Duan Y, Tan X, Lu X. Combinatory strategy for characterizing and understanding the ethanol synthesis pathway in cyanobacteria cell factories. Biotechnol Biofuels. 2015;8:184.
44. Ungerer J, Tao L, Davis M, Ghirardi M, Maness P-C, Yu J. Sustained photosynthetic conversion of CO_2 to ethylene in recombinant cyanobacterium *Synechocystis* 6803. Energy Environ Sci. 2012;5:8998–9006.
45. Kusakabe T, Tatsuke T, Tsuruno K, Hirokawa Y, Atsumi S, Liao JC, Hanai T. Engineering a synthetic pathway in cyanobacteria for isopropanol production directly from carbon dioxide and light. Metab Eng. 2013;20:101–8.
46. Khetkorn W, Incharoensakdi A, Lindblad P, Jantaro S. Enhancement of poly-3-hydroxybutyrate production in *Synechocystis* sp. PCC 6803 by overexpression of its native biosynthetic genes. Bioresour Technol. 2016;214:761–8.
47. Vayenos D, Romanos GE, Papageorgiou GC, Stamatakis K. *Synechococcus elongatus* PCC7942: a cyanobacterium cell factory for producing useful chemicals and fuels under abiotic stress conditions. Photosynth Res. 2020;146:235–45.
48. Du W, Liang F, Duan Y, Tan X, Lu X. Exploring the photosynthetic production capacity of sucrose by cyanobacteria. Metab Eng. 2013;19:17–25.
49. Guo Q, Hu H, Zhou Y, Yan Y, Wei X, Fan X, Yang D, He H, Oh Y, Chen K, et al. Glucosamine induces increased musclin gene expression through endoplasmic reticulum stress-induced unfolding protein response signaling pathways in mouse skeletal muscle cells. Food Chem Toxicol. 2019;125:95–105.
50. Krishnan A, McNeil BA, Stuart DT. Biosynthesis of fatty alcohols in engineered microbial cell factories: advances and limitations. Front Bioeng Biotechnol. 2020. https://doi.org/10.3389/fbioe.2020.610936.
51. Wang W, Liu X, Lu X. Engineering cyanobacteria to improve photosynthetic production of alka(e)nes. Biotechnol Biofuels. 2013;6:69.
52. Golden SS, Brusslan J, Haselkorn R. Genetic engineering of the cyanobacterial chromosome. Methods Enzymol. 1987;153:215–31.
53. Sinetova MA, Červený J, Zavřel T, Nedbal L. On the dynamics and constraints of batch culture growth of the cyanobacterium *Cyanothece* sp. ATCC 51142. J Biotechnol. 2012;162:148–55.
54. Ritchie RJ. Consistent sets of spectrophotometric chlorophyll equations for acetone, methanol and ethanol solvents. Photosynth Res. 2006;89:27–41.
55. Wellburn AR. The spectral determination of chlorophylls *a* and *b*, as well as total carotenoids, using various solvents with spectrophotometers of different resolution. J Plant Physiol. 1994;144:307–13.
56. Kim D, Langmead B, Salzberg SL. HISAT: a fast spliced aligner with low memory requirements. Nat Methods. 2015;12:357–60.
57. Li B, Dewey CN. RSEM: accurate transcript quantification from RNA-Seq data with or without a reference genome. BMC Bioinformatics. 2011;12:323.
58. Xin B, Tao F, Wang Y, Liu H, Ma C, Xu P. Coordination of metabolic pathways: enhanced carbon conservation in 1,3-propanediol production by coupling with optically pure lactate biosynthesis. Metab Eng. 2017;41:102–14.
59. Wang L, Feng Z, Wang X, Wang X, Zhang X. DEGseq: an R package for identifying differentially expressed genes from RNA-seq data. Bioinformatics. 2010;26:136–8.
60. Liu R, Hong J, Xu X, Feng Q, Zhang D, Gu Y, Shi J, Zhao S, Liu W, Wang X, et al. Gut microbiome and serum metabolome alterations in obesity and after weight-loss intervention. Nat Med. 2017;23:859–68.

Publisher's Note